


Transformation Dynamics in Origami

Chang Liu and Samuel M. Felton*

Northeastern University, Boston, Massachusetts 02115, USA

 (Received 27 June 2018; revised manuscript received 12 November 2018; published 20 December 2018)

A single origami crease pattern can be folded into many different structures from the flat-unfolded state, effectively transforming in shape and function. This makes origami engineering a promising approach to transforming machines, but predicting and controlling this transformation is difficult because the fundamental dynamics of origami systems at the flat-unfolded state are not well understood. Working with Miura-inspired mechanisms, we identify and validate a model to predict configuration switching in mechanical origami systems. The model incorporates a hidden degree of freedom introduced by material compliance in the Miura mechanism. We characterize this pseudojoint statically and dynamically to identify its lumped stiffness and inertia and use it to create a new dynamic model. This model can be used to predict which configuration an origami mechanism will settle in by balancing the kinetic and potential energy of the system. We apply this model to design a branching origami structure with 17 distinct configurations controlled by a single actuator and demonstrate reliable switching between these configurations with tailored dynamic inputs. Given the fact that origami can replicate almost any shape, we expect that this framework will be applicable to transformation in arbitrary structures and mechanisms.

DOI: [10.1103/PhysRevLett.121.254101](https://doi.org/10.1103/PhysRevLett.121.254101)

Introduction.—Origami-inspired mechanisms have multiple strengths, including tunable mechanical properties [1,2], transforming geometries [3,4], and ease of manufacturing [5,6]. Many of these traits have been formalized into mathematical- [7,8] and physics-based [9,10] models, enabling applications such as space deployment [11,12], microscale manufacturing [13], and computational fabrication [14]. Once folded, an ideally rigid origami mechanism is constrained to a limited set of trajectories, but when the mechanism is in the flat-unfolded state, it is in a kinematic singularity. From this point, the mechanism can bifurcate into two or more configurations, each with a distinct shape and kinematic behavior, by changing the directions of its folds [referred to collectively as the mountain-valley (MV) assignment] [15]. In physical specimens, the crease pattern is usually fixed during fabrication, but the MV assignment can be changed, presenting a practical approach to transformation.

Forcing a mechanism into a particular configuration can be challenging. Many systems use low-profile actuators, known as self-folding hinges [16,17], but it can be expensive or difficult to control multiple actuators at every hinge. Another option is to use a single actuator to dynamically excite the mechanism into a particular MV assignment [18]. To reliably achieve a desired MV assignment, we need a dynamic model that predicts the MV assignment from the flat-unfolded state. In this Letter, we present such a model for origami mechanisms that incorporates speed, position, and material stiffness.

Existing models of origami dynamics are built on the assumption that a fold pattern is equivalent to a set of rigid

linkages connected by rotary joints and, like other linkage systems, has a limited number of degrees of freedom (d.o.f.) [19]. However, preliminary results indicate that compliance in the facets and hinges leads to additional degrees of freedom, including in nominally 0-d.o.f. systems [20], resulting in higher-order dynamics. This challenge is compounded by the fact that MV transformation occurs around the flat-unfolded state. Since this state is a kinematic singularity and the system bifurcates at this point, rigid-linkage models cannot predict the system's behavior.

In this Letter, we study Miura-inspired structures as archetypal origami mechanisms [11]. The fold pattern is a tessellation of identical vertices, each with four creases. Two of these (referred to as the spinal creases) are collinear when flat and another two (called the peripheral creases) are symmetric across the spine with a peripheral angle α between the spinal and peripheral creases [Fig. 1(a)]. The lower and upper spinal creases are folded to angles θ_1 and θ_2 , respectively. An ideal mechanism (in which the facets are completely rigid) can enter two configurations from the flat-unfolded state, each with a single degree of freedom, so the state can be fully defined by θ_1 . When the spinal creases fold in the same direction, the spinal creases remain collinear and $\theta_1 = \theta_2$; when they fold in opposite directions, the spinal creases are offset by a segment angle ϕ and $\theta_1 = -\theta_2$. We call these the parallel [Fig. 1(b)] and antiparallel [Fig. 1(c)] configurations, respectively.

We observed additional “hidden” degrees of freedom resulting from bending modes in the facets, as well as stretching and off-axis twisting at the creases [1,20,21]. When a torque is applied to the Miura mechanism between

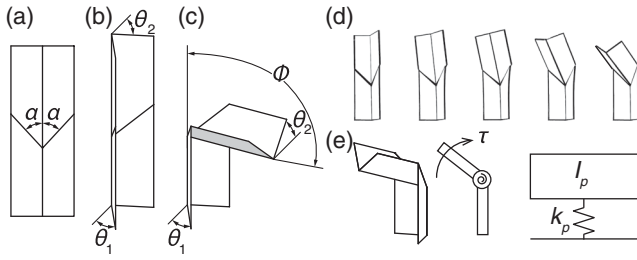


FIG. 1. (a) The Miura crease pattern can enter two configurations from the flat-unfolded state. (b) In the parallel configuration, the lower spinal angle θ_1 is equal to the upper spinal angle θ_2 . (c) In the antiparallel configuration $\theta_1 = -\theta_2$, and the upper spinal segment rotates to an angle ϕ relative to the lower segment. (d) In mechanical systems, the Miura pattern can bend at the vertex even when θ_1 is fixed and switch between configurations by passing through the flat position. (e) The extra degree of freedom can be modeled as a pseudojoint at the vertex between the two segments with a lumped-parameter stiffness and inertia.

the two segments, the upper segment will deflect, changing θ_2 and ϕ [Fig. 1(d)]. These deflections can be lumped into a single pseudojoint at the vertex [Fig. 1(e)]. The pseudojoint allows the upper segment of the mechanism (the two plates adjacent to the upper spinal crease) to move independently of the lower segment (the plates adjacent to the lower spinal crease). Therefore, we redefine our configurations as parallel when $\text{sgn}(\theta_1) = \text{sgn}(\theta_2)$ and antiparallel when $\text{sgn}(\theta_1) = -\text{sgn}(\theta_2)$.

Characterization of pseudojoint stiffness.—To characterize the lumped stiffness of the pseudojoint, we constructed Miura mechanisms with plastic facets and flexural hinges and applied a point force to the upper spinal crease while holding θ_1 fixed. The resulting torque to the pseudojoint was measured as a function of ϕ for three different values of θ_1 (15° , 25° , and 40°) [Fig. 2(a)].

As θ_1 increases, the stiffness of the pseudojoint increases about the stable equilibrium points $\theta_2 = \pm\theta_1$ and unstable

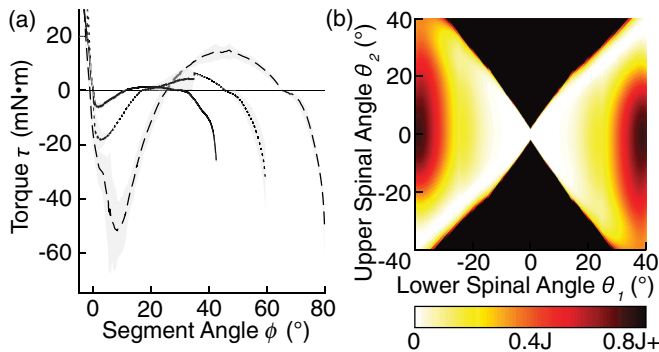


FIG. 2. “Pseudojoint” stiffness. (a) The vertex stiffness was characterized by measuring the torque as a function of the segment angle ϕ when θ_1 was fixed at different values. [$\theta_1 = 15^\circ$ (solid), 25° (dotted), 40° (dashed)]. Shaded region indicates standard deviation, $N = 3$. (b) Potential energy of the vertex as a function of θ_1 and θ_2 .

equilibrium at $\theta_2 = 0^\circ$. We repeated these experiments, while varying hinge stiffness and facet thickness, and observed that hinge stiffness has a substantial effect on pseudojoint stiffness, while facet thickness has a minor effect (Supplemental Material, Fig. S1 [22]).

We used these measurements to extrapolate the potential energy V in the mechanism as a function of θ_1 and θ_2 [Fig. 2(b)] by integrating the torque τ along the displacement ϕ (see Supplemental Material [22]),

$$V(\theta_1, \theta_2) = \int_{\phi_0}^{\phi_u} \tau(\phi) d\phi, \quad (1)$$

where ϕ_u is the angle corresponding to given angles θ_1 and θ_2 , and ϕ_0 corresponds to the point where $\theta_2 = \theta_1$. The potential energy plot shows there is a local energy minimum when $\theta_1 = \pm\theta_2$ and a local maximum when $\theta_2 = 0^\circ$. These regimes correspond to points of stable and unstable equilibrium, respectively (Supplemental Material, Fig. S2 [22]). Similar bistable behavior has previously been observed in multilayer Miura structures [23,24].

Characterization of pseudojoint dynamics.—To observe the dynamics of this mechanism, we applied pulse inputs with a magnitude of input speed ω_s to the lower spine velocity to approximate a step input of θ_1 from a start angle $\theta_0 = 40^\circ$ to a stop angle θ_s at 15° or 25° (Fig. 3) (see Supplemental Material [22]). During these experiments, we observed lag and oscillation in θ_2 characteristic of an underdamped second-order system [Figs. 4(a) and 4(b), Fig. S3, and Video S1]. To model this behavior, we developed a lumped-parameter model consisting of two parameters: the stiffness k_p and inertia I_p of the pseudojoint [22]. k_p was determined by linearizing the stiffness data in Fig. 2(a) and Fig. S1,

$$k_p = \begin{cases} \left. \frac{d\tau(\phi)}{d\phi} \right|_{\theta_2=\theta_1} & \text{when parallel} \\ \left. \frac{d\tau(\phi)}{d\phi} \right|_{\theta_2=-\theta_1} & \text{when antiparallel.} \end{cases} \quad (2)$$

Based on our stiffness measurements, this assumption is reasonable for small-amplitude oscillations because there is a linear stiffness regime when $\theta_2 \approx \pm\theta_1$, but it is inaccurate as θ_2 approaches 0° (Fig. S2). The inertia I_p of the upper segment was calculated from the geometry, material properties, and kinematic equations of the Miura mechanism by first calculating the inertia of the plates around the spinal hinge I_θ , corresponding to displacement of θ , and the plate inertia rotating around the vertex I_ϕ , corresponding to displacement of ϕ ,

$$I_p = \begin{cases} I_\theta & \text{when parallel} \\ I_\phi + I_\theta \left(\frac{\partial \theta}{\partial \phi} \right)^2 & \text{when antiparallel,} \end{cases} \quad (3)$$

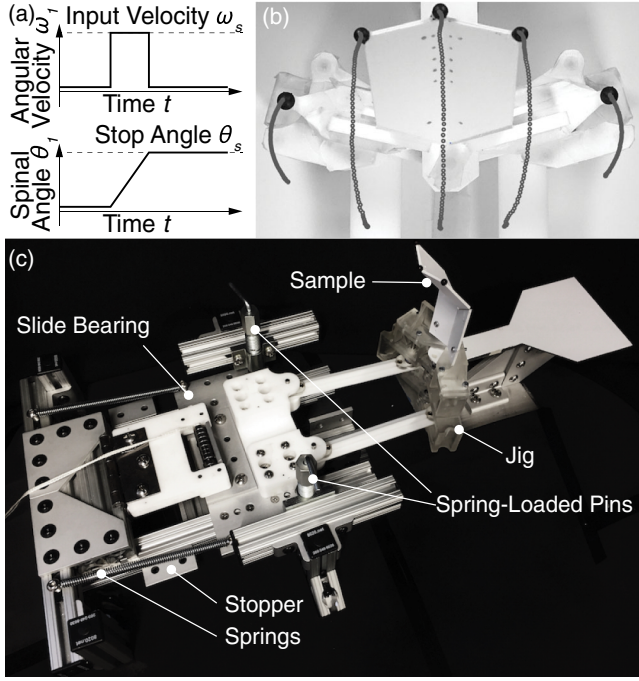


FIG. 3. Experimental setup to test the dynamic response of Miura mechanisms. (a) The input approximates a pulse input to the lower spine velocity of magnitude ω_s to a certain stop angle θ_s . (b) We measured θ_2 and ϕ by tracking five black markers. (c) We tested the dynamic behavior of the Miura mechanism by installing it in this experimental test bed that actuated the lower spinal crease through a spring-driven slide. Spring-loaded pins braked actuation at the stop angle.

These parameters are dependent on θ_1 and the system configuration, so we repeated this experiment with different combinations of ω_s , θ_s , and starting configuration. We compared the natural frequency $\sqrt{k_p/I_p}$ predicted by our model with the measured frequency and found that our predictions fell within 10% of the measured results (Table I).

Transformation criteria: We observed that, as the system settled, θ_2 would asymptotically approach a resting position at either θ_1 or $-\theta_1$, conforming to one of the two

configurations. Under certain conditions, such as slower input speeds, θ_2 would always remain on one side of the flat position [$\theta_2(t) \neq 0 \forall t$] and the configuration would not change [Fig. 4(a) and Figs. S3(a), S3(c), S3(g), S3(i), and S3(j)]. However, in other cases, such as faster speeds, θ_2 would cross the flat position ($\theta_2 = 0^\circ$) and settle on the opposite side that it started, representing transformation [Fig. 4(b) and Figs. S3(b), S3(d), and S3(h)]. As the system approaches the flat position, it becomes increasingly non-linear, making the linear approximation inaccurate.

We hypothesize that transformation occurs when the kinetic energy T of the upper segment is greater than the potential energy V at $\theta_2 = 0^\circ$. This represents when the system has enough kinetic energy to cross the strain energy local maximum and settle in the configuration on the other side. Because the potential energy is correlated with stiffness and kinetic energy is correlated with mass and speed, stiffer and slower mechanisms are less likely to transform, while heavier and faster structures are more likely to transform. We performed 93 experiments consisting of single trials with a different combination of θ_s , ω_s , starting configuration, hinge width, and facet thickness (Supplemental Material, Data S1 [22]). We calculated T from the angular velocities $\dot{\theta}_2$ and $\dot{\phi}$ so that $T = (I_\theta \dot{\theta}_2^2 + I_\phi \dot{\phi}^2)/2$ [22]. Some of the parameter combinations were tested three times, and in each set of experiments with identical parameters, transformation occurred in all trials or none of them, demonstrating the repeatability of this approach [Figs. 4(a), 4(b), 4(d), and 4(e) and Fig. S3].

Figure 4(c) plots each of these experiments with a diagonal line indicating where the kinetic energy equals the potential energy. In 90 out of 93 experiments, the mechanism transformed when $T > V$ and did not when $T < V$, validating our hypothesis. In the three remaining cases, $T \approx V$, and we expect that the error is due to damping in the system, which we neglected. Subsets of this data are plotted in Fig. S4 to differentiate the effect of the various parameters on T and V .

Mechanism passing through the flat-unfolded state: We extend this model to predict transformation when the

TABLE I. Experimental parameters and results of step input experiments.

Related figure	4(a)	4(b)	S3(a)	S3(b)	S3(c)	S3(d)	S3(g)	S3(h)	S3(i)	S3(j)
Speed ω_s (rad/s)	7.8	14.6	9.5	38.7	9.5	38.7	2.5	12.6	8.2	11.8
Stop angle θ_s ($^\circ$)	15	15	15	15	15	15	15	15	25	25
After transition:										
Configuration [parallel (P), antiparallel (AP)]	AP	P	P	AP	P	AP	AP	P	AP	AP
Stiffness k_p (mN m/rad)	57.5	843.0	843.0	57.5	843.0	57.5	57.5	843.0	101.1	101.1
Inertia I_p (mg m ⁴)	13.0	12.7	12.7	13.0	12.7	12.0	13.0	12.7	13.1	13.1
Modeled natural frequency (rad/s)	66.6	258.1	258.1	66.6	258.1	66.6	66.6	258.1	87.8	87.8
Experimental natural frequency (rad/s)	71.9	265.4	274.2	59.8	263.0	59.8	73.4	252.9	92.2	82.5
Natural frequency percent error (%)	8	3	6	10	2	10	10	2	5	6

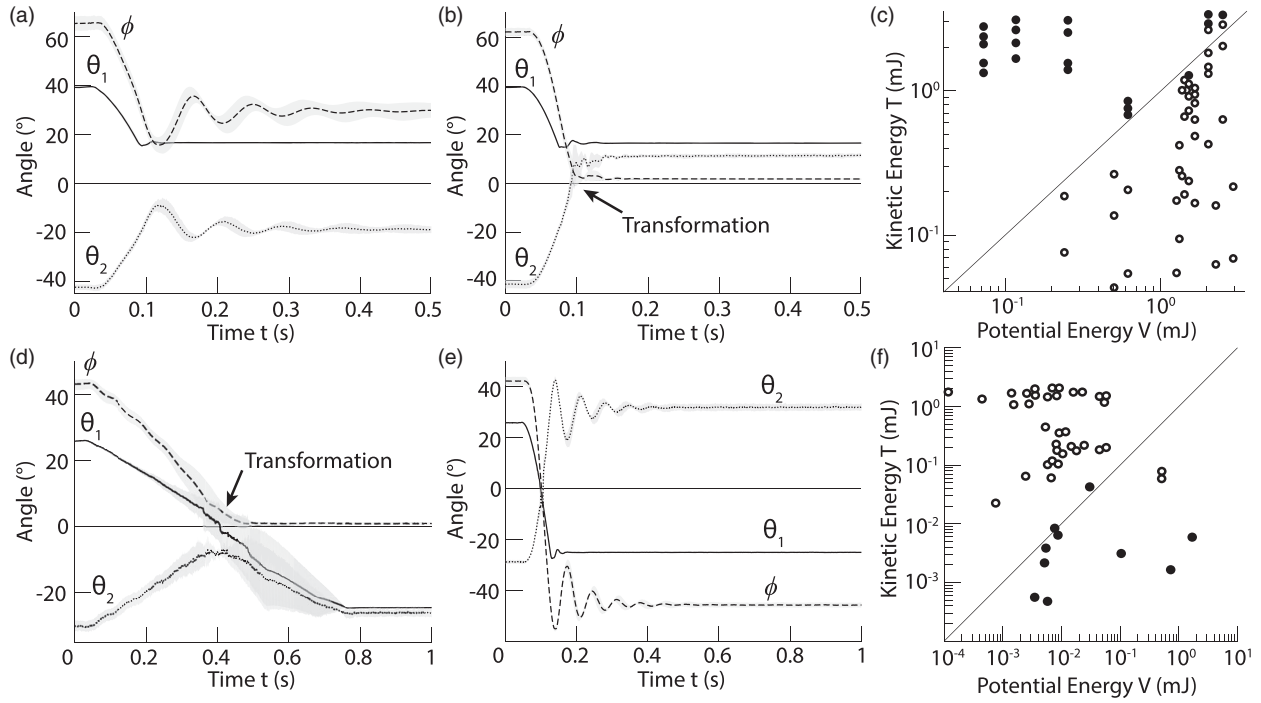


FIG. 4. Dynamic behavior of the Miura vertex. θ_1 (solid), θ_2 (dotted), and ϕ (dashed) are plotted after a step input to the lower spinal angle, shaded region indicates standard deviation, $N = 3$. (a) When actuated at a low speed ($\omega_s = 7.8$ rad/s), it remains in the starting configuration. (b) When actuated at a higher speed ($\omega_s = 14.6$ rad/s), it transforms. (c) Ninety-three experiments are plotted as a function of their kinetic energy T and potential energy V . Transformations are plotted as black dots, nontransforming experiments as white dots, and the line indicates $T = V$. (d) When the mechanism is actuated at a low speed ($\omega_s = 1.2$ rad/s) through the flat-unfolded state, it transforms. (e) At higher speeds ($\omega_s = 13.7$ rad/s), it remains in the starting configuration. (f) Forty-six experiments, in which the mechanism passes through the flat state, are plotted as a function of T and V .

mechanism passes through the flat-unfolded state. We performed similar pulse input experiments in which $\theta_0 = 25^\circ$ and $\theta_s = -25^\circ$. Because of the phase lag between θ_1 and θ_2 (Fig. 4) there is a “window” in which transformation can occur when θ_1 has crossed the flat state and θ_2 has not, and the size of this window is dependent on the pseudojoint stiffness. In these experiments, θ_1 is crossing the origin, so θ_2 must also cross the origin for the mechanism to stay in the same configuration. Therefore, we expect that a system in which $T < V$ transforms [Fig. 4(d) and Fig. S5(c)] and a system in which $T > V$ does not [Fig. 4(e) and Fig. S5(d)]. We compared T and V in 46 different trials and this model accurately predicted transformation in 42 of them [Fig. 4(f) and Data S2]. We observed that this model was less accurate in part because strain energy was stored in the mechanism as it passed through the flat position, changing the energy balance at the transition point. We expect that a more detailed dynamic model would have a greater predictive accuracy, but the current model is sufficient for identifying reliable transformation patterns.

Implementation in a multiconfiguration mechanism.— We built a branching origami structure consisting of five Miura vertices to show that this approach to transformation applies to vertices in series and in parallel (Fig. S6). This

device has 17 nontrivial configurations [Fig. 5(a) and Fig. S7]. The branches have different facet masses and hinge stiffnesses so that each vertex has a different pseudojoint stiffness and inertia, breaking the dynamic symmetry the mechanism.

The branching origami mechanism was actuated at a fixed speed of approximately 3.4 rad/s from a starting position of 40° to an arbitrary stop angle and then back to 40° . Eight different stop angles (16° , 13° , 10° , 7° , -27° , -30° , -40° , and -45°) were used to create eight distinct actuation signals, and these signals were applied to transform the mechanism between configurations (Fig. 5 and Fig. S8). Fifty-eight repeatable transformations (from one specific configuration to another in response to a specific input) were identified and tested ten times (Table S1) with a 100% success rate. A sample of these are shown in Video S2 to illustrate the process.

We applied the model to each vertex in the branching structure, accounting for additional factors not seen in the single vertex experiments, including gravity and linear momentum (Tables S2 and S3). The model correctly predicted 88% of the vertex configurations [22]. These results show that the model can be applied to multivertex systems, but also indicate challenges in modeling multivertex systems. The majority of inaccurate predictions were

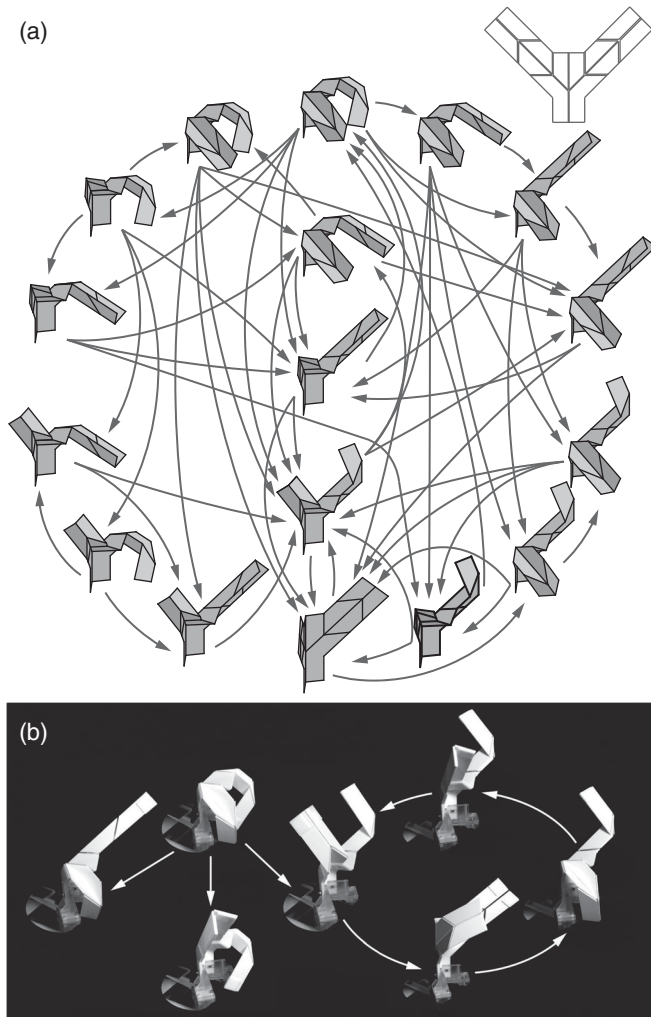


FIG. 5. Transformation of a branching origami mechanism with five Miura vertices. This device has 17 nontrivial configurations, and the pseudojoint stiffness and inertia of each vertex is tailored to have different transformation criteria. (a) A graph showing all 58 repeatable transformations that we identified. (b) A sample of the different transformation paths that the mechanism can take.

due to a small subset of transformations, suggesting that there are systemic factors we are not accounting for, such as configuration-dependent coupling between vertices (Tables S4 and S5).

Conclusion.—These results demonstrate that reliable origami transformation can be accomplished with a single actuator. Compared to distributed self-folding [25], transformation by dynamic excitation has the potential to reduce costs and control complexity and transformation time. Unlike previous examples of origami machines that harness facet compliance [26], the transformation is discrete and, aside from the transition point, the mechanism generally behaves according to the direct kinematic model. The branching mechanism results indicate that the model reasonably captures reconfiguration of multivertex patterns. Future work could improve the model by investigating

coupling between vertices, using nonlinear techniques to model multiple pseudojoints in series and system bifurcations to model configuration switching. We expect that future work will also generalize this transformation technique to apply to vertices with more than four creases by introducing additional hidden degrees of freedom to the vertex.

This work was funded by Northeastern University.

*s.felton@northeastern.edu

- [1] J. L. Silverberg, A. A. Evans, L. McLeod, R. C. Hayward, T. Hull, C. D. Santangelo, and I. Cohen, *Science* **345**, 647 (2014).
- [2] J. T. Overvelde, T. A. De Jong, Y. Shevchenko, S. A. Begera, G. M. Whitesides, J. C. Weaver, C. Hoberman, and K. Bertoldi, *Nat. Commun.* **7**, 10929 (2016).
- [3] E. Hawkes, B. An, N. M. Benbernou, H. Tanaka, S. Kim, E. D. Demaine, D. Rus, and R. J. Wood, *Proc. Natl. Acad. Sci. U.S.A.* **107**, 12441 (2010).
- [4] S.-J. Kim, D.-Y. Lee, G.-P. Jung, and K.-J. Cho, *Sci. Robotics* **3**, eaar2915 (2018).
- [5] N. Bassik, G. M. Stern, and D. H. Gracias, *Appl. Phys. Lett.* **95**, 091901 (2009).
- [6] C. D. Onal, M. T. Tolley, R. J. Wood, and D. Rus, *IEEE/ASME Trans. Mechatron.* **20**, 2214 (2015).
- [7] E. D. Demaine and J. O'Rourke, *Geometric Folding Algorithms: Linkages, Origami, Polyhedra* (Cambridge University Press, Cambridge, England, 2007).
- [8] E. D. Demaine and T. Tachi, in *LIPICs-Leibniz International Proceedings in Informatics* (Schloss Dagstuhl-Leibniz-Zentrum fuer Informatik, 2017), Vol. 77.
- [9] M. Schenk and S. D. Guest, *Origami* **5**, 291 (2011).
- [10] C. Qiu, V. Aminzadeh, and J. S. Dai, *J. Mech. Design* **135**, 111004 (2013).
- [11] K. Miura, *Inst. Space Astronaut. Sci. Rep.* **618**, 1 (1985).
- [12] S. A. Zirbel, R. J. Lang, M. W. Thomson, D. A. Sigel, P. E. Walkemeyer, B. P. Trease, S. P. Magleby, and L. L. Howell, *J. Mech. Design* **135**, 111005 (2013).
- [13] J. Rogers, Y. Huang, O. G. Schmidt, and D. H. Gracias, *MRS Bull.* **41**, 123 (2016).
- [14] A. M. Mehta and D. Rus, in *Robotics and Automation (ICRA), 2014 IEEE International Conference on* (IEEE, 2014), pp. 1460–1465.
- [15] B. G.-g. Chen and C. D. Santangelo, *Phys. Rev. X* **8**, 011034 (2018).
- [16] J. K. Paik and R. J. Wood, *Smart Mater. Struct.* **21**, 065013 (2012).
- [17] S. M. Felton, M. T. Tolley, B. Shin, C. D. Onal, E. D. Demaine, D. Rus, and R. J. Wood, *Soft Matter* **9**, 7688 (2013).
- [18] F. Zuliani, C. Liu, J. Paik, and S. M. Felton, *IEEE Rob. Autom. Lett.* **3**, 1426 (2018).
- [19] H. Fang, S. Li, H. Ji, and K. W. Wang, *Phys. Rev. E* **95**, 052211 (2017).
- [20] J. L. Silverberg, J.-H. Na, A. A. Evans, B. Liu, T. C. Hull, C. D. Santangelo, R. J. Lang, R. C. Hayward, and I. Cohen, *Nat. Mater.* **14**, 389 (2015).

- [21] J. A. Faber, A. F. Arrieta, and A. R. Studart, *Science* **359**, 1386 (2018).
- [22] See Supplemental Material at <http://link.aps.org/supplemental/10.1103/PhysRevLett.121.254101>, for materials and methods.
- [23] S. Li and K. W. Wang, *J. R. Soc. Interface* **12**, 20150639 (2015).
- [24] S. Li, H. Fang, and K. W. Wang, *Phys. Rev. Lett.* **117**, 114301 (2016).
- [25] S. Felton, M. Tolley, E. Demaine, D. Rus, and R. Wood, *Science* **345**, 644 (2014).
- [26] S. M. Felton, D.-Y. Lee, K.-J. Cho, and R. J. Wood, in *IEEE International Conference on Robotics and Automation (ICRA), 2014* (IEEE, 2014), pp. 2913–2918.